Integrated strain and force feedback for high-performance control of piezoelectric actuators

Andrew J. Fleming [a,*], Kam K. Leang [b]

[a] School of Electrical Engineering and Computer Science, University of Newcastle, Callaghan, NSW 2308, Australia
[b] Mechanical Engineering, University of Nevada – Reno, Reno, NV 89557, USA

ARTICLE INFO

ABSTRACT

This paper presents a new sensor arrangement and feedback controller for hysteresis, creep and vibration in piezoelectric actuators. A piezoelectric force sensor is combined with a resistive strain gage to provide both extremely low noise and high stability. The use of a force sensor also results in a system transfer function that exhibits zero-pole ordering. Such systems allow a simple integral controller to provide excellent tracking and damping performance with guaranteed stability.

The proposed technique is demonstrated on a nanopositioning platform with a range of 10 μm and a resonance frequency of 2.4 kHz. In closed-loop, the controller damps the resonance by 33 dB and provides a tracking bandwidth of 1.8 kHz. Excellent tracking of a 130 Hz triangular reference and reduction of hysteresis to 0.46% at 10 Hz is also demonstrated. The closed-loop positioning noise, predicted from the sensor noise density, was approximately 0.67 nm peak-to-peak, or 0.0067% of the 10 μm range.

© 2010 Elsevier B.V. All rights reserved.

1. Introduction

Due to their high stiffness, compact size and effectively infinite resolution, piezoelectric actuators are universally employed in a wide range of scientific and industrial applications. Examples include nanofabrication systems [1–4], fiber aligners [5], beam scanners [6], nanopositioning systems [7], and scanning probe microscopes [8–10].

Unfortunately, piezoelectric actuators cannot be directly applied in positioning applications as they exhibit a significant amount of hysteresis over large ranges and creep at low-frequencies [11,7]. These effects can cause tracking error in excess of 20%. As a result, many applications require some form of feedback [12] or feedforward control [13] to reduce or eliminate non-linearity.

The most popular technique for control of piezoelectric actuated systems is sensor-based feedback control with an integral or proportional-integral controller. This approach is simple, robust to modeling error, and effectively reduces non-linearity at low-frequencies. However, the bandwidth of such systems is severely limited by low gain-margin [12]. It can be shown that the maximum closed-loop bandwidth is equal to the product of twice the damping ratio ξ and natural frequency ω_n [14], that is,

$$\text{max closed-loop bandwidth} < 2\omega_n\xi. \tag{1}$$

This is a severe limitation as the damping ratio is usually in the order of 0.01, so the maximum closed-loop bandwidth is less than 2% of the resonance frequency. Techniques aimed at improving the closed-loop bandwidth are based on either inversion of resonant dynamics using a notch filter [15] or a damping controller [16–19]. Damping controllers are less sensitive to variations in resonance frequency than inversion-based controllers but an integral tracking loop is still required. This inevitably results in low stability margins and instability if the resonance frequency is sufficiently reduced. In addition, the greater bandwidth of damping and inversion-based controllers increases the amount of positioning noise.

To demonstrate the limitations imposed by sensor noise, consider a nanopositioner with feedback control derived from a capacitive sensor with a noise density of 20 pm/$\sqrt{\text{Hz}}$. An estimate of the RMS position noise can be found from the noise density and square-root of closed-loop bandwidth,

$$\text{RMS noise} = \sqrt{3.14 \times \text{bandwidth}} \times \text{noise density}, \tag{2}$$

where 3.14 is a correction factor to convert the 3 dB bandwidth of a first-order system to an equivalent noise bandwidth. For example, with a closed-loop bandwidth of 1.8 kHz, the positioning noise is 1.5 nm RMS. If the noise is normally distributed, the 6σ peak-to-peak noise will be approximately 10 nm.

* Corresponding author. Tel.: +61 2 4921 6493; fax: +61 2 4921 6993.
E-mail addresses: andrew.fleming@newcastle.edu.au (A.J. Fleming),
kam@unr.edu (K.K. Leang).
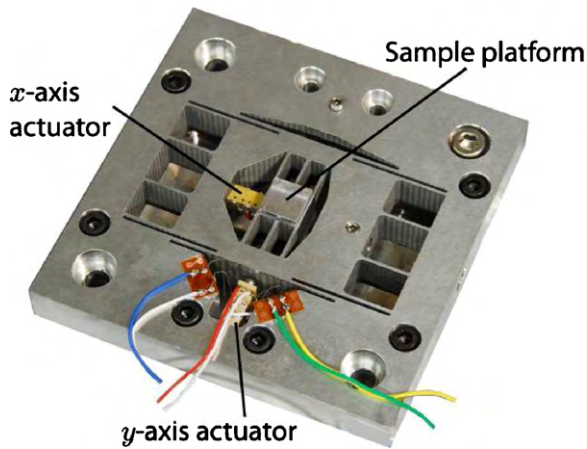
Fig. 1. High-speed nanopositioning platform with strain and force sensors fitted to the y-axis actuator.

Fig. 2. A piezoelectric actuator with integrated strain and force sensors. The strain sensors are bonded to the front and back surface while the force sensor is a small piezoelectric stack placed between the actuator and load ball. The load half-ball is used to eliminate the transmission of torsion and bending moments to the force sensor and moving platform.
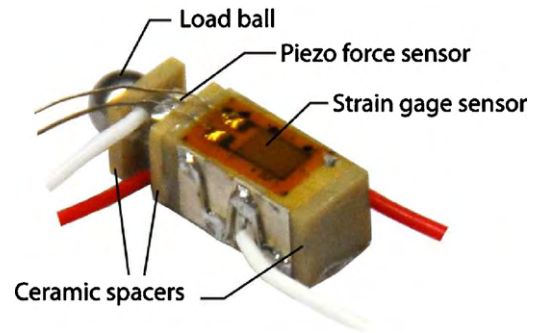
Feedforward control [20,21] can be used independently [22,23] or to improve the response of a feedback system without increasing the positioning noise [12,24]. However, feedforward control may not be feasible if variations in resonance frequency are expected [25]. Additionally, feedforward compensation of creep and hysteresis requires an accurate model, one that may be complex and computationally demanding to procure and invert. If the reference signal is periodic, iterative feedforward [26,27], adaptive [28], and repetitive control [29] can be applied. These techniques can provide excellent tracking performance but require a periodic reference and significant digital signal processing capabilities.

In this work, a new technique is presented for control of hysteresis, creep and vibration in piezoelectric actuated systems. The proposed technique utilizes a resistive strain gage and piezoelectric force sensor to estimate displacement. The piezoelectric force sensor exhibits extremely low noise at frequencies above 1 Hz but cannot measure static displacement and is prone to drift. To eliminate these low-frequency errors, the strain gage signal is substituted at low frequencies. In contrast to standard capacitive, inductive and optical displacement sensors, the proposed scheme can be integrated into the actuator which minimizes parts count and overall system cost. The total cost of parts and components for the proposed scheme is less than $100, which is considerably less than the typical cost of a capacitive sensor, which is approximately $2000.

In Section 2, a nanopositioning system is described for demonstration of the proposed technique. This is followed by an introduction to strain and piezoelectric force sensors in Sections 3 and 4. Section 4 also contains the derivation of an electromechanical model and a review of the recently introduced technique of force feedback position control [14]. This technique is extended in Section 5 for use with complementary strain and force sensors. Due to the system properties, a simple integral controller can provide excellent tracking and damping performance with guaranteed stability. This technique is demonstrated in Section 6. Conclusions are drawn in Section 7.

2. Experimental system

Although the technique of strain and force feedback is applicable to a wide range of mechatronic systems, in this work, the proposed controller is applied to the nanopositioning platform pictured in Fig. 1. This platform is designed for high-bandwidth applications such as video-speed scanning probe microscopy [30–33]. The platform develops approximately 10 μm of travel in the lateral scan axes and 4 μm travel in the vertical direction. As the vertical and x-axes are physically small with low mass, the resonance frequencies are greater than 10 kHz. However, due to the large y-axis mass, the resonance frequency in this direction is only 2.4 kHz. As this axis is required to follow triangular trajectories up to 100 Hz, compensation is required to eliminate oscillation and reduce nonlinearity. The technique of strain and force feedback will be applied to achieve high-performance tracking with simplicity, low-cost and high robustness.

The actuator used to drive the y-axis is pictured in Fig. 2. It comprises of a 10 mm Noliac SCMAP07 actuator connected serially to a 2 mm Noliac CMAP06 stack force sensor. The ceramic spacers provide a robust bonding surface between the two stacks and minimize the measurement error due to Poisson coupling. This error is caused by contraction of the stack body during elongation. If the sensor is bonded directly to the actuator, this contraction is erroneously measured and produces an effect opposite in polarity to the applied force. A further discussion of Poisson coupling and methods to eliminate it can be found in reference [14]. In addition to the force sensor, there are also two resistive strain sensors attached to the top and bottom surface of the actuator. Full descriptions of the strain gages, instrumentation, and force sensor are provided in Sections 3 and 4. A Kaman inductive position sensor (SMU9000-15N) was also used to measure the frequency and time domain displacement of the system. These open-loop responses are plotted in Section 6.

The actuator was driven with a Piezodrive PDL200 linear amplifier. With the 330 nF actuator capacitance, the PDL200 provides a bandwidth of approximately 22 kHz. The amplifier gain and other system sensitivities are summarized in Fig. 3.
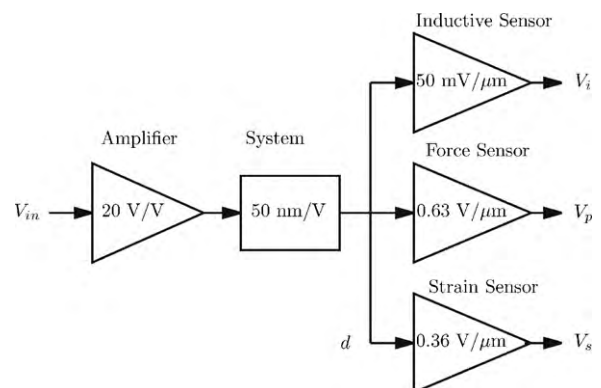
Fig. 3. System gains and sensitivities.
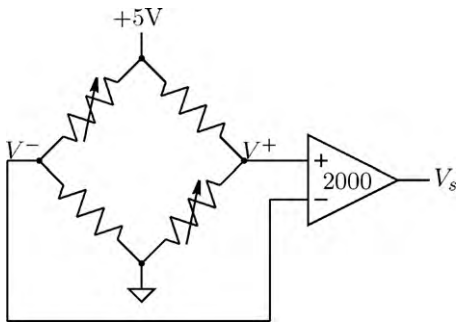
Fig. 4. Strain gage bridge circuit. The two strain gages are the varying elements of the bridge, likewise the dummy resistors are fixed. All of the resistors have a nominal resistance of 350 Ω.

3. Resistive strain feedback

Resistive strain gages are the most common types of position sensor used for control of piezoelectric actuators. They are often integrated into the actuator for position feedback. Strain sensors can also be retrofitted to other actuators simply by bonding the sensor to the actuator surface. Two example applications that utilize resistive strain feedback are [34] and [35].

Resistive strain gages are constructed from a thin layer of conducting foil laminated between two insulating layers. With a zig-zag conductor pattern, strain gages can be designed for high sensitivity in only one direction, e.g. elongation. As a strain gage is elongated, the resistance increases proportionally. The change in resistance per unit strain is known as the gage factor GF defined by

$$GF = \frac{\Delta R/R_G}{\epsilon}, \tag{3}$$

where ΔR is the change in resistance from the nominal value R_G for a strain ϵ. As the gage factor is typically in the order of 1 or 2, the change is resistance is similar in magnitude to the percentage of strain. For a piezoelectric transducer with a maximum strain of approximately 0.1%, the change in resistance will also be around 0.1%. This small variation requires a bridge circuit for accurate measurement.

### 3.1. Practical application of strain gages

In Fig. 2, the piezoelectric actuator described in Section 2 is pictured with a strain gage bonded to each of the two non-electrode sides. The strain gages are Omega SGD-3/350-LY13 gages, with a nominal resistance of 350 Ω and package dimensions of 7 mm × 4 mm.

The electrical wiring of the strain gages is illustrated in Fig. 4. The full bridge circuit is completed by two dummy 350 Ω wire wound resistors and excited by a 5 V DC source. The differential bridge voltage ($V^+ - V^-$) is acquired and amplified by a Vishay Micro-Measurements 2120B strain gage amplifier. As the circuit is a two-varying-element full-bridge, the measured voltage is

$$V_s = \frac{A_v V_b}{2}\left(\frac{\Delta R}{R_G + \Delta R/2}\right), \tag{4}$$

where $A_v = 2000$ is the differential gain and $V_b = 5$ V is the excitation voltage. By substituting (3) into (4) and neglecting the small bridge non-linearity,[1] the measured voltage is proportional to the

[1] In a two-varying-element bridge circuit, the non-linearity due to $\Delta R/2$ in Eq. (4) is 0.5% non-linearity per percent of strain [36]. Since the maximum strain of a piezoelectric actuator is 0.1%, the maximum non-linearity is only 0.05% and can be neglected. If this magnitude of non-linearity is not tolerable, compensating circuits are available [36].
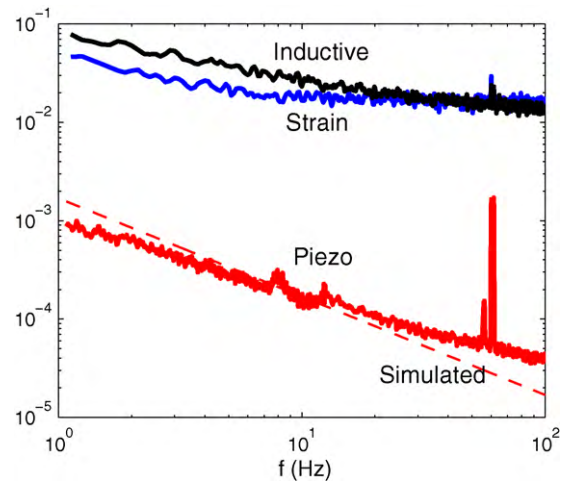
Fig. 5. The noise density of the inductive, resistive strain, and piezoelectric force sensor, all scaled to nm/$\sqrt{\text{Hz}}$. The simulated noise of the piezoelectric force sensor is also plotted as a dashed line.

strain ϵ and displacement d by

$$V_s = GF\frac{1}{2}A_v V_b \epsilon \tag{5}$$

$$V_s = GF\frac{1}{2L}A_v V_b d, \tag{6}$$

where L is the actuator length. With a gage factor of 1, the position sensitivity of the strain sensor will be 0.5 V/μm which implies a full scale voltage of 5 V for the maximum strain of 10 μm.

By calibrating the strain gage output with the inductive sensor, the experimental sensitivity was found to be 0.3633 V/μm.

3.2. Strain gage characteristics and noise

Compared to other position sensors, strain gages are compact, low-cost, precise, and highly stable—particularly in the four-varying-element configuration that requires two actuators in a push–pull arrangement [34]. However, a major disadvantage is the significant measurement noise. This is due to the high instrumentation gain, the thermal noise of the sensor, and the voltage and current noise of the amplifier. As a result, strain gages usually exhibit an order of magnitude greater noise density than capacitive or inductive sensors.

The noise density of the strain signal (scaled to nm) is plotted in Fig. 5. The sensor exhibits a constant noise density of approximately 20 pm/$\sqrt{\text{Hz}}$ and a $1/f$ noise corner frequency of around 10 Hz. This is comparable to the inductive sensor which has a range of 200 μm. However, for an inductive or capacitive sensor with a range of 10 μm, the expected noise density would be only 1 pm/$\sqrt{\text{Hz}}$, which is an order of magnitude less than the resistive strain gage. Hence, strain gages are rarely used in systems designed for high resolution. If they are utilized in such systems, the closed-loop bandwidth must be severely restrained. For example, with a noise density of 20 pm/$\sqrt{\text{Hz}}$, the closed-loop bandwidth must be less than 22 Hz to achieve a peak-to-peak noise of 1 nm (assuming a Gaussian distribution and first-order response). To overcome this difficulty, a low noise force sensor is described in the following section.

4. Force feedback

Force feedback was recently proposed as a new technique for vibration control and linearization of nanopositioning systems [14]. Rather than using a direct position sensor, this technique uses a measurement of the actuator load force as shown in Fig. 6(a).
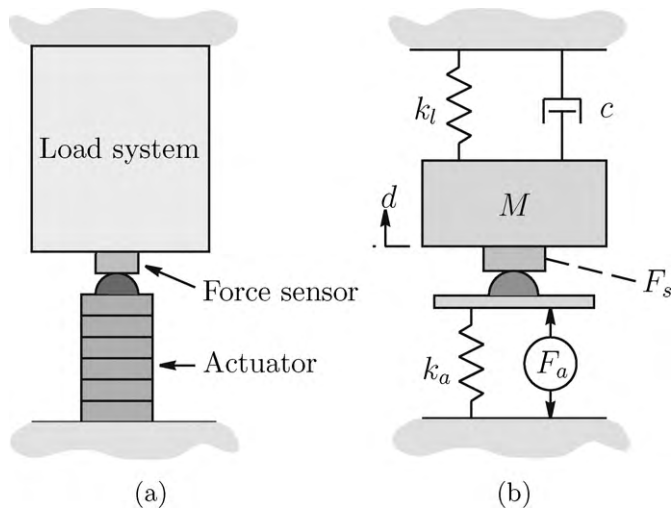
Fig. 6. A piezoelectric actuator driving a load system (a). The mechanical equivalent diagram with a single-degree-of-freedom load system (b).

Although the load force F_s can be measured in a number of ways, in this application it is desirable to minimize the additional mass and compliance associated with the sensor. In such scenarios, piezoelectric transducers are an excellent choice. They provide high sensitivity and bandwidth with low noise at high frequencies. In Fig. 2, a small Noliac CMAP06 stack actuator is glued to the end of the main actuator for use as a force sensor. Other types of piezoelectric force sensor include discrete plate sensors and integrated stack sensors [14]. The sensitivity and characteristics of piezoelectric force sensors are discussed in the following two subsections.

In Section 4.3, a simple model of the experimental system is derived. This is shown diagrammatically in Fig. 6. Although force feedback can be applied to a wide class of systems, the load system is modeled as a simple spring-mass system. Although this model is simple, it adequately represents the dominant dynamics exhibited by the experimental system and many other positioning systems. The extension to higher order systems is trivial and will be discussed in Section 5.1.

4.1. Piezoelectric actuator and sensor modeling

It has been shown previously that a piezoelectric actuator can be modeled as a force generator F_a and stiffness k_a [14]. This representation is shown in Fig. 6(b). The generated force and associated spring constant are

$$F_a = d_{33}nk_aV_a, \qquad k_a = \frac{c^E A}{L}, \tag{7}$$

where d_{33} is the piezoelectric charge constant [11], n is the number of layers, V_a is the applied voltage, c^E is Young's modulus of elasticity, A is the cross-sectional area, and L is the actuator length. The ratio of developed force to applied voltage is $d_{33}nk_a$ (N/V, Newtons per Volt). In the following, this constant will be denoted as g_a, where

$$F_a = g_aV_a, \quad \text{and} \quad g_a = d_{33}nk_a.$$

Piezoelectric actuators can also be used as force sensors. If the transducer electrodes are left open-circuit or connected to a high-impedance buffer, the generated charge is deposited on the transducers internal capacitance. The open-circuit voltage of a piezoelectric force sensor is

$$V_s = \frac{nd_{33}}{C}F_s, \tag{8}$$
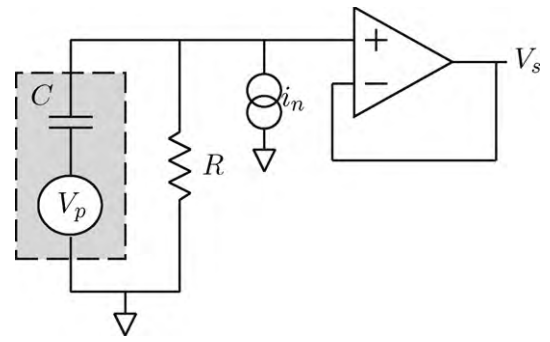
Fig. 7. The electrical model of a piezoelectric force sensor. The open-circuit voltage V_p is high-pass filtered by the transducer capacitance C and leakage resistance R. The current source i_n represents the current noise of a high-impedance buffer.

where C is the transducer capacitance defined by $C = n\epsilon_T A/h$ and A, h and ϵ_T are the area, layer thickness and dielectric permittivity under constant stress. The scaling factor between force and measured voltage is nd_{33}/C (V/N). In the following, this sensor constant will be denoted as g_s, where

$$V_s = g_sF_s, \quad \text{and} \quad g_s = \frac{nd_{33}}{C}. \tag{9}$$

4.2. Force sensor characteristics and noise

Due to the high mechanical stiffness of piezoelectric force sensors, thermal or Boltzmann noise is negligible compared to the electrical noise arising from interface electronics. As piezoelectric sensors have a capacitive source impedance, the noise density $N_{V_s}(\omega)$ of the sensor voltage V_s is due primarily to the current noise i_n generated by the interface electronics. The equivalent electrical circuit of a piezoelectric sensor and high-impedance buffer is shown in Fig. 7. Neglecting the leakage resistance R, the noise density of the sensor voltage is

$$N_{V_s}(\omega) = i_n\frac{1}{C\omega}, \tag{10}$$

where N_{V_s} and i_n are the noise densities of the sensor voltage and current noise, measured in Volts and A/$\sqrt{\text{Hz}}$ respectively.

The experimentally measured noise density of the piezoelectric force sensor is plotted in Fig. 5. The predicted noise density is also plotted. The sensor has a capacitance is 30 nF, and the voltage buffer (OPA606) has a noise density of 2 fA/$\sqrt{\text{Hz}}$.

In Fig. 5 the superior noise performance of the piezoelectric sensor is evident. The noise density is more than 2 orders of magnitude lesser than the strain and inductive sensors at 100 Hz. The noise density also continues to reduce at higher frequencies. However, at low-frequencies the noise of the piezoelectric force sensor will eventually surpass the other sensors. As the noise density is equivalent to an integrator excited by white noise, the measured voltage will drift around at low-frequencies. A time record that illustrates this behavior is plotted in Fig. 8. The large drift amplitude is clearly evident. Thus, although the piezoelectric force sensor generates less noise than the strain and inductive sensors at frequencies in the Hz range and above, it is inferior at frequencies below approximately 0.1 Hz.

In addition to noise, piezoelectric force sensors are also limited by dielectric leakage and finite buffer impedance at low-frequencies. The induced voltage V_p shown in Fig. 7 is high-pass filtered by the internal transducer capacitance C and the leakage resistance R. The cut-off frequency is

$$f_{hp} = \frac{1}{2\pi RC} \text{ Hz}. \tag{11}$$
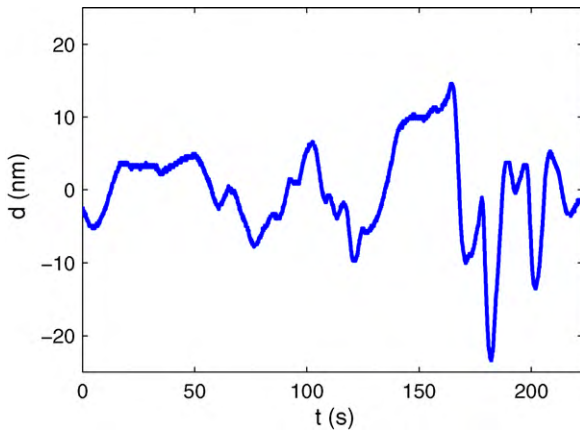
Fig. 8. Low-frequency noise of a piezoelectric force sensor scaled to nanometers. The peak-to-peak noise over 220 s is 38 nm or 26 mV.

The buffer circuit used in this work has an input impedance of 100 MΩ, this results in a low-frequency cut-off of 0.05 Hz. To avoid a phase lead of more than 6°, the piezoelectric force sensor cannot be used to measure frequencies less than 0.5 Hz.

4.3. Mechanical dynamics

The simplified model of a single-degree-of-freedom positioning system is shown in Fig. 6(b). The model contains two components: the actuator, modeled as a force generator F_a and stiffness k_a; and the load system, modeled as a mass M and stiffness k_l with damping c. The actuator mass is assumed to be negligible. The displacement of the load system d can be found by applying Newton's second law,

$$M\ddot{d} = F_a - k_a d - k_l d - c\dot{d},\tag{12}$$

As the stiffness of the actuator and load act in parallel, the total stiffness k experienced by the load mass is $k = k_a + k_l$. The equation of motion is then

$$M\ddot{d} + kd + c\dot{d} = F_a,\tag{13}$$

and the transfer function from actuator force F_a to platform displacement d is

$$\frac{d}{F_a} = \frac{1}{Ms^2 + cs + k}.\tag{14}$$

Including the actuator gain, the transfer function from applied voltage to displacement can be written

$$G_{dV_a} = \frac{d}{V_a} = \frac{g_a}{Ms^2 + cs + k}\tag{15}$$

The load force F_s is also of interest, this can be related to the actuator force F_a by summing the forces acting on the force sensor,

$$F_a = k_a d - F_s.\tag{16}$$
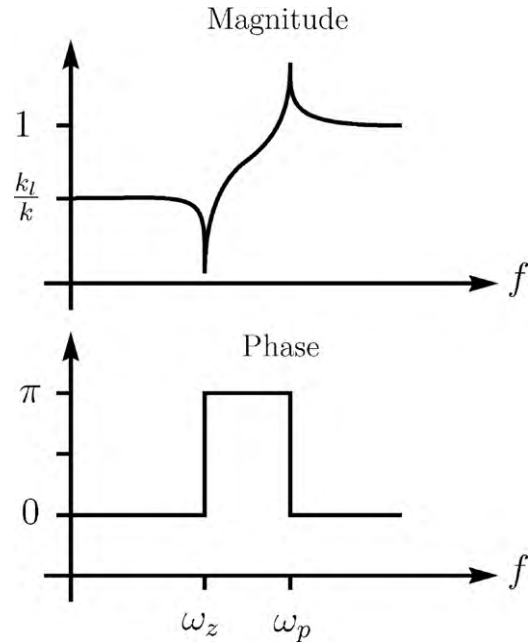
This results in the following transfer function between the applied force F_a and measured force F_s,

$$\frac{F_s}{F_a} = 1 - k_a \frac{d}{F_a}\tag{17}$$

$$\frac{F_s}{F_a} = \frac{Ms^2 + cs + k_l}{Ms^2 + cs + k}.\tag{18}$$

By including the actuator and sensor gains g_a and g_s, the system transfer function from the applied voltage to measured voltage can be found,

$$G_{V_sV_a} = \frac{V_s}{V_a} = g_a g_s \frac{Ms^2 + cs + k_l}{Ms^2 + cs + k}.\tag{19}$$

Fig. 9. Magnitude and phase response of F_s/F_a (17).

The relationship between the measured force and displacement can also be found by applying Newton's second law to the platform mass or by multiplying (18) and the inverse of (14). By including the force sensor gain, the measured voltage V_s is related to displacement by

$$\frac{V_s}{d} = g_s(Ms^2 + cs + k_l).\tag{20}$$

Thus, the displacement is proportional to force up until the frequency $\omega_z = \sqrt{k_l/M}$. The sensitivity is $g_s k_l$ (V/m). At frequencies above ω_z, the measured force is proportional to platform acceleration [14].

4.4. System poles and zeros

This transfer function $G_{V_sV_a}$ (19) consists of a pair of resonant poles and zeros at frequencies ω_z and ω_p,

$$\omega_z = \sqrt{\frac{k_l}{M}}, \quad \omega_p = \sqrt{\frac{k}{M}} = \sqrt{\frac{k_a + k_l}{M}}.\tag{21}$$

The frequency of the system zeros will always be lower than the poles. This characteristic is shown in the frequency response of F_s/F_a in Fig. 9. For systems with multiple degrees-of-freedom, it can be shown that the zero-pole pattern repeats for each resonance mode. This is discussed in more detail in Section 5.1.

4.5. Integral Force Feedback (IFF)

The feedback diagram of an integral force feedback controller is shown in Fig. 10. The loop consists of the plant $G_{V_sV_a}$ and an integral
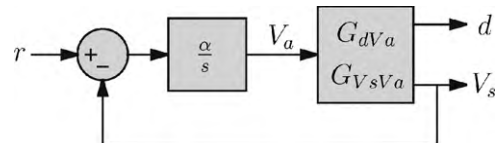
Fig. 10. The system $G_{V_sV_a}$ controlled by an Integral Force Feedback (IFF) controller $C(s) = \frac{\alpha}{s}$.
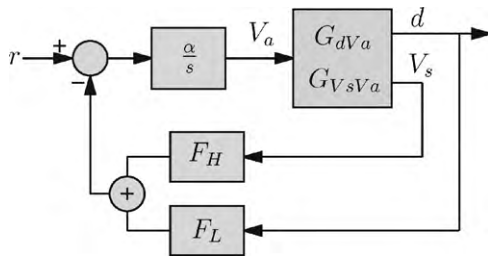
Fig. 11. Dual sensor feedback loop that utilizes a strain gage measurement below 10 Hz and the piezoelectric force measurement above 10 Hz.

controller

$$C(s) = \frac{\alpha}{s}. \tag{22}$$

A key property of the system $G_{V_sV_a}$ is that the phase response lies between $0°$ and $180°$. This is a general feature of flexible structures with a collocated actuator and force measurement [37]. Another unique property of such systems is that integral control can be applied directly. This is due to the phase characteristics of the loop-gain. As the integral controller has a constant phase lag of $90°$, the total loop-gain phase ($\angle C(j\omega)G_{V_sV_a}(j\omega)$) lies between $-90°$ and $90°$. This implies that the closed-loop system has an infinite gain-margin and phase-margin of $90°$. The robustness and simplicity are two outstanding properties of systems with integral force feedback.

A solution for the optimal feedback gain α for maximum damping has already been derived in reference [37]. These results were adapted for the system considered here in reference [14]. Assuming the system damping is small, the optimal feedback gain $\alpha^\star$ is [14]

$$\alpha^\star = \frac{\omega_p \sqrt{\omega_p/\omega_z}}{g_s g_a}. \tag{23}$$

Additional expressions for the maximum closed-loop damping and pole locations can be found in reference [14]. In practice, where only an identified model may be available, the optimal gain $\alpha^\star$ can be found numerically from the root-locus [14]. This approach is taken in Section 6.

The closed-loop transfer functions from the reference voltage to the displacement and measured force, $\widehat{G_{dr}}$ and $\widehat{G_{V_sr}}$, are

$$\widehat{G_{dr}} = \frac{CG_{dV_a}}{1 + CG_{V_sV_a}}. \tag{24}$$

$$\widehat{G_{V_sr}} = \frac{CG_{V_sV_a}}{1 + CG_{V_sV_a}}. \tag{25}$$

With integral force feedback the position is regulated indirectly by controlling the load force F_s. The closed-loop position sensitivity can be determined from (24) to be $1/g_s k_l$ (m/V).

5. Strain and force feedback

In Section 3 resistive strain gages were discussed as a method for position control of piezoelectric actuators. It was concluded that strain gages are too noisy for high-bandwidth positioning applications. In contrast, piezoelectric force sensors have excellent noise performance at frequencies in the Hz range and above. In addition, the use of a force sensor results in a system that can be easily controlled with excellent bandwidth and stability margins.

To overcome the low-frequency noise and phase-lead exhibited by the piezoelectric sensor, the strain gage can be utilized as a complementary sensor. Such an arrangement is illustrated in Fig. 11. This control loop is similar to Fig. 10 except for the additional complementary filters F_H and F_L. These complementary filters substitute the displacement measurement d for V_s at frequencies below the crossover frequency f_c. As the force measurement contains a

parasitic high-pass filter at 0.05 Hz, f_c is chosen to be 10 Hz. At this frequency the phase error of the force sensor is less than $0.5°$. The simplest choice of complementary filters are

$$F_H = g_H \frac{s}{s + 2\pi f_c} \quad \text{and} \quad F_L = g_L \frac{2\pi f_c}{s + 2\pi f_c}. \tag{26}$$

where g_H and g_L are the gains used to equate the sensitivity of d and V_s. In practice, it is convenient to choose g_H and g_L so that the sensitivity from V_a to each sensor signal is unity. This approach is taken in the experimental results.

If the gains g_H and g_L are included in $G_{V_sV_a}$ and G_{dV_a}, respectively, the closed-loop response $\widehat{G_{dr}}$ is

$$\widehat{G_{dr}} = \frac{G_{dV_a}C}{1 + CG_{V_sV_a}}. \tag{27}$$

As this control loop is unconditionally stable, there is no restriction on the controller gain. However, α was chosen in the

(a) Displacement G_{dr} $(\theta m /V)$

(b) Force G_{V_sr} (V/V)
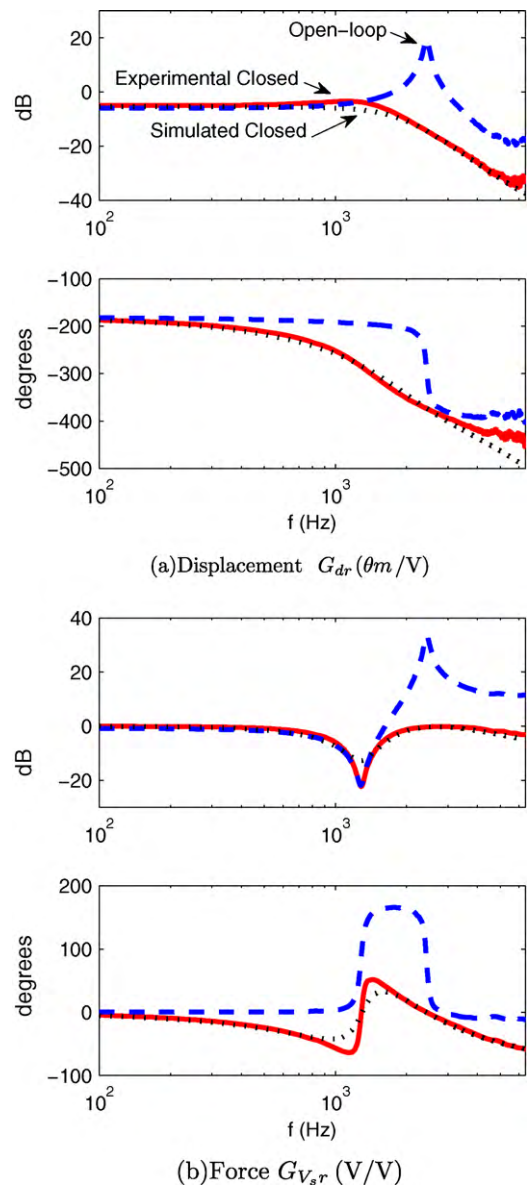
Fig. 12. The experimental open- and closed-loop frequency responses (dashed and solid line). The open-loop responses are measured from the amplifier input to the inductive sensor output and force sensor voltage. The closed-loop responses are measured from the reference voltage to the same outputs. The simulated closed-loop response is also plotted (dotted line).
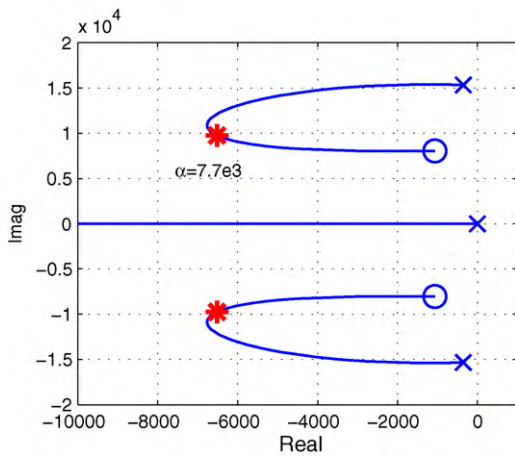
Fig. 13. Root-locus of the closed-loop poles. The optimal gain of α = 7700 corresponds to a damping ratio of 0.557.
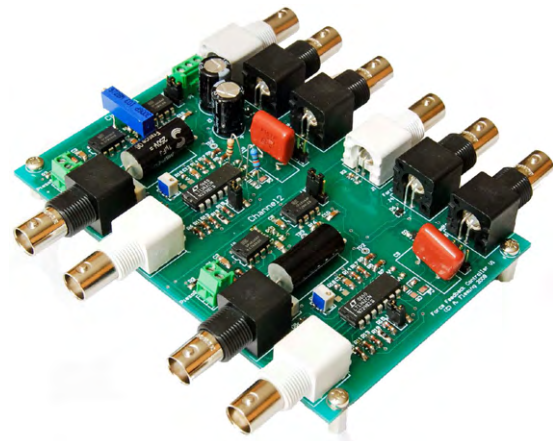

Fig. 14. A two channel controller board containing high-impedance buffers, complementary filters, and two force feedback controllers.

previous section to provide optimal damping performance, this value should be retained. Further increases in α are not productive as the disturbance rejection at the resonance frequency will degrade.

As the piezoelectric sensor noise is negligible compared to the strain gage, and the crossover frequency f_c is significantly less than the closed-loop bandwidth, the closed-loop position noise density of the dual sensor controller can be approximated by

$$\widehat{N_d}(\omega) = \left| F_L(j\omega) \right| N_d(\omega), \tag{28}$$

where $\widehat{N_d}$ is the closed-loop noise density and $N_d(\omega)$ is the noise density of the strain gage scaled to meters. Advantageously, the strain signal is filtered by F_L which has a much lower bandwidth than the complimentary sensitivity function, hence a large saving in position noise is realized.

If we assume that $N_d(\omega)$ is a constant N_d, the standard deviation σ (RMS value) of the positioning noise is

$$\sigma = N_d \sqrt{3.14 f_c}, \tag{29}$$

where the factor 3.14 is the effective noise bandwidth for a first order system. For the strain gages discussed in Section 3.2, the noise density is approximately $20 \, \text{pm}/\sqrt{\text{Hz}}$, this implies a positioning noise of 0.11 nm RMS for a bandwidth of 10 Hz, and a 6σ peak-to-peak noise of approximately 0.67 nm. It is important to note that this calculation only considers sensor-induced noise and also assumes a Gaussian distribution. Hence the calculation is approximate but useful as an indication of closed-loop noise under controlled conditions.

5.1. Higher order modes

So far, only a single-degree-of-freedom system has been considered. Although this is appropriate for modeling the first resonance mode, it does not capture the higher order modes that occur in distributed mechanical systems. However, such higher order modes are not problematic as they do not disturb the zero-pole ordering of the transfer function from applied actuator voltage to the measured force.

In reference [38] it is shown that the transfer function of a generalized mechanical system with a discrete piezoelectric transducer and collocated force sensor is guaranteed to exhibit zero-pole ordering. That is, the transfer function $G_{V_s V_a}$ will always exhibit zero-pole ordering. As the zero-pole ordering of the system is guaranteed, it follows that the controller discussed in Section 4.5

will also guarantee the stability of systems with multiple modes. The zero-pole ordering of an experimental system with multiple modes, and its successful control using integral force feedback was reported in reference [14].
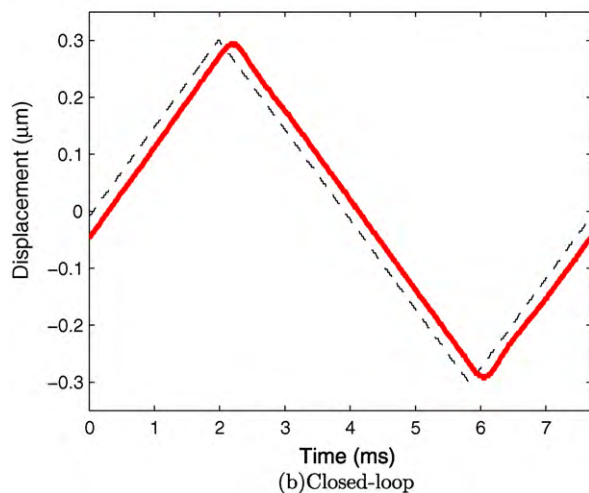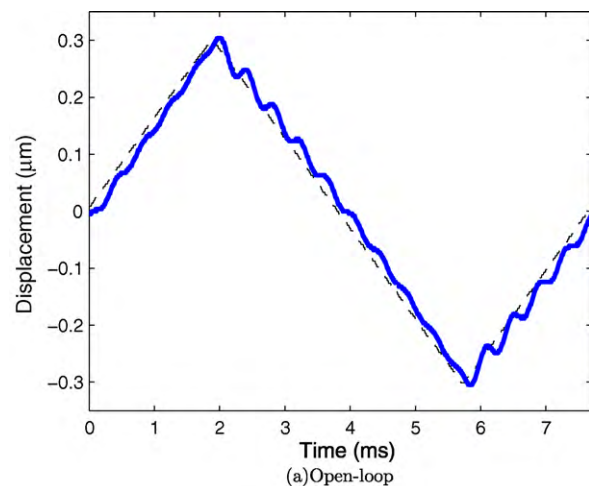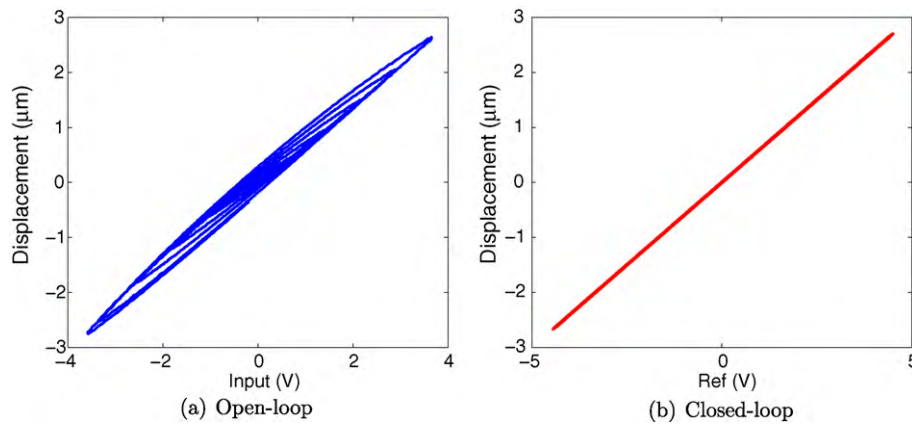

Fig. 15. The open- and closed-loop response to a 600 nm peak-to-peak 130 Hz triangle wave. The RMS deviation-from-linear over a half period was 10 nm RMS in open-loop and 1.9 nm RMS in closed-loop. The maximum peak-to-peak error over 90% of a half period was 45 nm in open-loop (a) and 6.7 nm in closed-loop (b).

Fig. 16. The open- and closed-loop response of the system to a 10 Hz sine-wave ramped from 0 to 150 V peak-to-peak. The maximum error due to hysteresis is reduced from 460 nm (8.5%) in open-loop (a) to 25 nm (0.46%) in closed-loop (b).

6. Experimental results

As the integral force feedback controller has only one parameter, an approximately optimal gain can be found from only frequency response data. However, to plot the closed-loop pole locations and find a numerically optimal gain, a model is required. For this purpose, a second-order single-input two-output model was procured using the frequency domain subspace technique[2][39]. The open-loop data used to procure the model is plotted in Fig. 12.

The root-locus of the closed-loop system is plotted in Fig. 13. The optimal gain was found numerically to be $\alpha = 7700$. With this gain, the controller was implemented on an electronics board designed to implement all of the functions required by a force feedback system.[3] This includes a high-impedance buffer for the force sensor, the complementary filters, and the controller transfer function (Fig. 14).

The experimental closed-loop frequency responses are plotted in Fig. 12. The closed-loop responses exhibit excellent damping performance (-33 dB) and a closed-loop positioning bandwidth of 1.8 kHz. This is exceptional considering that the open-loop resonance frequency is 2.4 kHz. Also plotted are the simulated closed-loop frequency responses which closely agree with experimental results.

In Fig. 15 the time domain performance of the force feedback controller is demonstrated by comparing the open- and closed-loop responses to a 130 Hz triangle wave. The controller effectively eliminates oscillation and reduces the deviation-from-linear from 45 nm in open-loop to 6.7 nm in closed-loop. The tracking-lag was not included in the error calculation as this is eliminated in practical applications by a phase-lead in either the applied reference, or the recorded data. If real-time elimination of tracking-lag is required, an additional feedforward controller is required [20,21].

Due to the integral tracking action and wide feedback bandwidth, the controller is also effective at reducing dynamic hysteresis. In Fig. 16, the 8.5% error due to hysteresis in open-loop is reduced to 0.46% in closed-loop. It is also of interest to examine the closed-loop response to creep non-linearity. As the control-loop-gain at frequencies where creep occurs is extremely large, the open-loop error of 9.7% after 50 s is no longer measurable in closed-loop. If the piezoelectric force sensor was used alone without a strain gage, as in [14], there would be no feedback at low-frequencies and the performance in respect to creep and
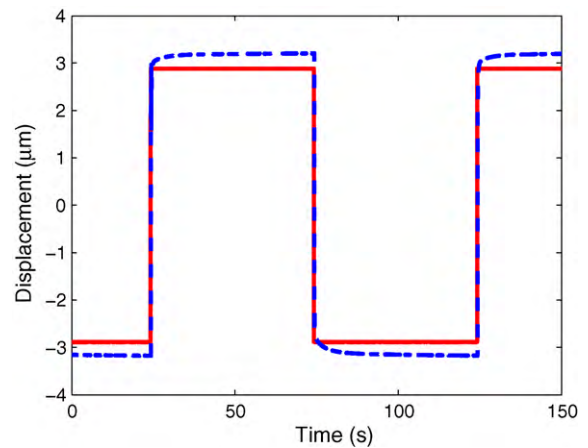
Fig. 17. The creep behavior exhibited by the actuator in open-loop (dashed line) and closed-loop (solid line). The input was a 196 V square with a period of 100 s. In open-loop, the error due to creep was 560 nm peak-to-peak or 9.7% of the peak-to-peak displacement. Due to the high control gain at low-frequencies, creep was not detectable in closed-loop.

low-frequency hysteresis would resemble the open-loop response (Fig. 17).

7. Conclusions

This paper presents a new low-cost sensing and feedback scheme for reduction of creep, hysteresis and vibration in piezo-electric actuated systems. The technique of strain and force feedback utilizes a resistive strain gage and piezoelectric force sensor to measure displacement. A benefit of piezoelectric sensors is that they exhibit extremely low noise at frequencies in the Hz range and above. However, below 1 Hz, dielectric leakage introduces phase-lead, and current noise results in slow random drift. To eliminate these low-frequency errors, the strain gage signal is substituted at low frequencies. The strain gage and piezoelectric sensor signals are combined into a displacement estimate with a pair of first-order complementary filters. The resulting signal exhibits the low noise of a piezoelectric sensor and the stability of a resistive strain gage.

In addition to low noise, another benefit of the piezoelectric force sensor is the zero-pole ordering of the transfer function from applied actuator voltage to measured force. This allows a simple integral controller to provide excellent tracking and damping performance with guaranteed stability.

---

[2] A Matlab implementation of this algorithm is freely available by contacting the author.

[3] Circuit diagrams can be obtained by contacting the author.

The proposed technique of strain and force feedback was demonstrated on a high-speed nanopositioning platform. Due to simplicity, the controller was easily implemented with an analog circuit. The closed-loop frequency response demonstrated a 33 dB damping of the resonance peak and a closed-loop bandwidth of 1.8 kHz which is close to the open-loop resonance frequency of 2.4 kHz. In the time domain, excellent tracking of a 130 Hz triangle wave was achieved and hysteresis was reduced from 8.5% to 0.46% at 10 Hz. Although the strain gage contributes the majority of closed-loop positioning noise, the bandwidth of this signal is only 10 Hz. This resulted in a closed-loop noise of approximately 0.67 nm peak-to-peak which is 0.0067% of the 10 μm range.

Due to the low-cost of strain gages and piezoelectric sensors, and the simplicity of implementation, these results were achieved at a fractional cost of a traditional inductive or capacitive displacement sensor. Future work involves the inclusion of a feedforward controller to extend the bandwidth beyond the first resonance frequency.

Acknowledgements

References

[1] A. Ferreira, C. Mavroidis, Virtual reality and haptics for nanorobotics, IEEE Robotics and Automation Magazine 13 (3) (2006) 78–92.
[2] A.A. Tseng, S. Jou, A. Notargiacomo, T.P. Chen, Recent developments in tip-based nanofabrication and its roadmap, Journal of Nanoscience and Nanotechnology 8 (5) (2008) 2167–2186.
[3] A.A. Tseng (Ed.), Nanofabrication: Fundamentals and Applications, World Scientific, 2008.
[4] H.C. Liaw, B. Shirinzadeh, J. Smith, Sliding-mode enhanced adaptive motion tracking control of piezoelectric actuation systems for micro/nano manipulation, IEEE Transactions on Control Systems Technology 16 (4) (2008) 826–833.
[5] Z. Wang, L. Chen, L. Sun, An integrated parallel micromanipulator with flexure hinges for optical fiber alignment, in: Proceedings of the IEEE International Conference on Mechatronics and Automation, Harbin, China, 2007, pp. 2530–2534.
[6] B. Potsaid, J.T. Wen, M. Unrath, D. Watt, M. Alpay, High performance motion tracking control for electronic manufacturing, Journal of Dynamic Systems, Measurement, and Control 129 (2007) 767–776.
[7] S. Devasia, E. Eleftheriou, S.O.R. Moheimani, A survey of control issues in nanopositioning, IEEE Transactions on Control Systems Technology 15 (5) (2007) 802–823.
[8] S.M. Salapaka, M.V. Salapaka, Scanning probe microscopy, IEEE Control Systems Magazine 28 (2) (2008) 65–83.
[9] D.Y. Abramovitch, S.B. Andersson, L.Y. Pao, G. Schitter, A tutorial on the mechanisms, dynamics, and control of atomic force microscopes, in: Proceedings of the American Control Conference, New York City, NY, 2007, pp. 3488–3502.
[10] E. Meyer, H.J. Hug, R. Bennewitz, Scanning Probe Microscopy. The Lab on a Tip, Springer-Verlag, Heidelberg, Germany, 2004.
[11] H.J.M.T.A. Adriaens, W.L. de Koning, R. Banning, Modeling piezoelectric actuators, IEEE/ASME Transactions on Mechatronics 5 (4) (2000) 331–341.
[12] K.K. Leang, S. Devasia, Feedback-linearized inverse feedforward for creep, hysteresis, and vibration compensation in AFM piezoactuators, IEEE Transactions on Control Systems Technology 15 (5) (2007) 927–935.
[13] D. Croft, G. Shed, S. Devasia, Creep, hysteresis, and vibration compensation for piezoactuators: atomic force microscopy application, ASME Journal of Dynamic Systems, Measures, and Control 123 (2001) 35–43.
[14] A.J. Fleming, Nanopositioning system with force feedback for high-performance tracking and vibration control, IEEE Transactions on Mechatronics 15 (3) (2010) 433–447.
[15] D.Y. Abramovitch, S. Hoen, R. Workman, Semi-automatic tuning of PID gains for atomic force microscopes, in: Proceedings of the American Control Conference, Seattle, WA, 2008, pp. 2684–2689.
[16] A.J. Fleming, S.O.R. Moheimani, Sensorless vibration suppression and scan compensation for piezoelectric tube nanopositioners, IEEE Transactions on Control Systems Technology 14 (1) (2006) 33–44.
[17] S.S. Aphale, B. Bhikkaji, S.O.R. Moheimani, Minimizing scanning errors in piezoelectric stack-actuated nanopositioning platforms, IEEE Transactions on Nanotechnology 7 (1) (2008) 79–90.
[18] A.J. Fleming, S.S. Aphale, S.O.R. Moheimani, A new method for robust damping and tracking control of scanning probe microscope positioning stages, IEEE Transactions on Nanotechnology, in press, doi:10.1109/TNANO.2009.2032418.
[19] A. Sebastian, A. Pantazi, S.O.R. Moheimani, H. Pozidis, E. Eleftheriou, A self servo writing scheme for a MEMS storage device with sub-nanometer precision, in: Proceedings of the IFAC World Congress, Seoul, Korea, 2008, pp. 9241–9247.
[20] S. Devasia, Review of feedforward approaches for nano precision positioning in high speed SPM operation, in: Proceedings of the IFAC World Congress, Seoul, Korea, 2008, pp. 9221–9229.
[21] K.K. Leang, Q. Zou, S. Devasia, Feedforward control of piezoactuators in atomic force microscope systems, Control Systems Magazine 29 (1) (2009) 70–82.
[22] R. Changhai, S. Lining, Hysteresis and creep compensation for piezoelectric actuator in open-loop operation, Sensors and Actuators A 122 (1) (2005) 124–130.
[23] H. Janocha, K. Kuhnen, Real-time compensation of hysteresis and creep in piezoelectric actuators, Sensors and Actuators A 79 (2) (1999) 83–89.
[24] J.A. Butterworth, L.Y. Pao, D.Y. Abramovitch, A comparison of control architectures for atomic force microscopes, Asian Journal of Control 11 (2) (2009) 175–181.
[25] S. Devasia, Should model-based inverse inputs be used as feedforward under plant uncertainty? IEEE Transactions on Automatic Control 47 (11) (2002) 1865–1871.
[26] K. Kim, Q. Zou, Model-less inversion-based iterative control for output tracking: piezo actuator example, in: Proceedings of the American Control Conference, Seattle, WA, 2008, pp. 2710–2715.
[27] Y. Li, J. Bechhoefer, Feedforward control of a piezoelectric flexure stage for AFM, in: Proceedings of the American Control Conference, Seattle, WA, 2008, pp. 2703–2709.
[28] S. Bashash, N. Jalili, Robust adaptive control of coupled parallel piezo-flexural nanopositioning stages, IEEE/ASME Transactions on Mechatronics 14 (1) (2009) 11–20.
[29] Y. Shan, K.K. Leang, Repetitive control with Prandtl-Ishlinskii hysteresis inverse for piezo-based nanopositioning, in: American Control Conference, St. Louis, MO, 2009.
[30] T. Ando, N. Kodera, T. Uchihashi, A. Miyagi, R. Nakakita, H. Yamashita, K. Matada, High-speed atomic force microscopy for capturing dynamic behavior of protein molecules at work, e-Journal of Surface Science and Nanotechnology 3 (2005) 384–392.
[31] G. Schitter, K.J. Åström, B.E. DeMartini, P.J. Thurner, K.L. Turner, P.K. Hansma, Design and modeling of a high-speed AFM-scanner, IEEE Transactions on Control Systems Technology 15 (5) (2007) 906–915.
[32] A.D.L. Humphris, M.J. Miles, J.K. Hobbs, A mechanical microscope: high-speed atomic force microscopy, Applied Physics Letters 86 (2005), 034106(1–3).
[33] M.J. Rost, L. Crama, P. Schakel, E. van Tol, G.B.E.M. van Velzen-Williams, C.F. Overgauw, H. ter Horst, H. Dekker, B. Okhuijsen, M. Seynen, A. Vijftigschild, P. Han, A.J. Katan, K. Schoots, R. Schumm, W. van Loo, T.H. Oosterkamp, J.W.M. Frenken, Scanning probe microscopes go video rate and beyond, Review of Scientific Instruments 76 (5) (2005), 053710(1–9).
[34] G. Schitter, P.J. Thurner, P.K. Hansma, Design and input-shaping control of a novel scanner for high-speed atomic force microscopy, Mechatronics 18 (5–6) (2008) 282–288.
[35] W. Dong, L.N. Sun, Z.J. Du, Design of a precision compliant parallel positioner driven by dual piezoelectric actuators, Sensors and Actuators A 135 (1) (2007) 250–256.
[36] W. Kester, Sensor Signal Conditioning, Analog Devices, 2002.
[37] A. Preumont, Mechatronics, Dynamics of Electromechanical and Piezoelectric Systems, Springer, 2006.
[38] A. Preumont, B. de Marneffe, A. Deraemaeker, F. Bossens, The damping of a truss structure with a piezoelectric transducer, Computers and Structures 86 (2007) 227–239.
[39] T. McKelvey, H. Akcay, L. Ljung, Subspace-based multivariable system identification from frequency response data, IEEE Transactions on Automatic Control 41 (7) (1996) 960–978.

Biographies

Andrew J. Fleming was born in Dingwall, Scotland in 1977. He graduated from The University of Newcastle, Australia (Callaghan campus) with a Bachelor of Electrical Engineering in 2000 and PhD in 2004. Dr. Fleming is presently an Australian Research Council fellow stationed at the School of Electrical Engineering and Computer Science, The University of Newcastle, Australia. His research includes nanopositioning, high-speed scanning probe microscopy, micro-cantilever sensors, and sensor-less control of sound and vibration. In 2007, Dr. Fleming was awarded the University of Newcastle Vice-Chancellors Award for Researcher of the Year. Also in 2007, Dr. Fleming was co-recipient of the IEEE Control Systems Society Outstanding Paper Award for research published in the *IEEE Transactions on Control Systems Technology*. Dr. Fleming is an Associate Editor of *Advances in Acoustics and Vibration*. He is the co-author of two books, several patent applications and more than 80 Journal and Conference papers.

Kam K. Leang received the BS and MS degrees in mechanical engineering from the University of Utah, Salt Lake City, in 1997 and 1999, respectively, and the PhD degree from the University of Washington, Seattle, in December 2004. He joined the Department of Mechanical Engineering, University of Nevada-Reno, in 2008. From 2005 to 2008, he taught in the Mechanical Engineering Department at Virginia Commonwealth University, Richmond. His research interests include modeling and control of piezoactuators for scanning probe microscopy applications, fabrication and control of electroactive polymers, mechatronics, and design of microelectromechanical systems (MEMS) for nanotechnology.